The Journal of Chemical Physics

Low energy electron impact resonances of anthracene probed by 2D photoelectron imaging of its radical anion

Cite as: J. Chem. Phys. **152**, 174303 (2020); https://doi.org/10.1063/5.0007470
Submitted: 13 March 2020 . Accepted: 12 April 2020 . Published Online: 04 May 2020

Golda Mensa-Bonsu, Aude Lietard, David J. Tozer, and Jan R. R. Verlet

The Journal of Chemical Physics ARTICLE scitation.org/journal/jcp

Low energy electron impact resonances of anthracene probed by 2D photoelectron imaging of its radical anion

Cite as: J. Chem. Phys. 152, 174303 (2020); doi: 10.1063/5.0007470
Submitted: 13 March 2020 • Accepted: 12 April 2020 •
Published Online: 4 May 2020

Golda Mensa-Bonsu, Aude Lietard, David J. Tozer, and Jan R. R. Verlet[a)]

AFFILIATIONS

Department of Chemistry, Durham University, Durham DH1 3LE, United Kingdom

[a)]Author to whom correspondence should be addressed: j.r.r.verlet@durham.ac.uk

ABSTRACT

Electron-molecule resonances of anthracene were probed by 2D photoelectron imaging of the corresponding radical anion up to 3.7 eV in the continuum. A number of resonances were observed in both the photoelectron spectra and angular distributions, and most resonances showed clear autodetachment dynamics. The resonances were assigned using density functional theory calculations and are consistent with the available literature. Competition between direct and autodetachment, as well as signatures of internal conversion between resonances, was observed for some resonances. For the 1^2B_{2g} resonance, a small fraction of population recovers the ground electronic state as evidenced by thermionic emission. Recovery of the ground electronic state offers a route of producing anions in an electron–molecule reaction; however, the energy at which this occurs suggests that anthracene anions cannot be formed in the interstellar medium by electron capture through this resonance.

I. INTRODUCTION

Polycyclic aromatic hydrocarbons (PAHs) are of interest because of their ubiquity in various research areas including medicinal chemistry, atmospheric sciences, combustion chemistry, astrochemistry, and molecular electronics.[1–5] Many of the important properties and uses of PAHs are linked to their electronic structure and the excited states for both their neutral and ionized species. In the context of the interstellar medium, PAHs are believed to represent a major store for carbon and have been implicated to contribute to the Diffuse Interstellar Bands (DIBs).[6–11] PAHs exist in regions where UV radiation and free electrons are abundant, making the formation of charged PAHs likely. In particular, there is a background of low-energy electrons that may lead to their capture by a neutral PAH to form the anion.[12–14] Such electron capture processes are mediated by electron–molecule resonances, which can form temporary negative ions. The competition between autodetachment (AD) and internal conversion dynamics of these resonances ultimately determines whether the ground electronic state of the anion or anionic products are formed. Consequently, the study of such electron–molecule resonances has been of considerable interest. Here, a frequency-resolved (2D) photoelectron (PE) imaging study of the anthracene radical anion, $C_{14}H_{10}^-$, characterizing the anion resonances that lie within the first 3.7 eV of the electron-neutral continuum, is presented.

Anthracene is the smallest linear PAH with a positive adiabatic electron affinity of 0.532(3) eV.[15] Experimentally, anion resonances can be probed either by electron scattering experiments such as electron transmission spectroscopy[16,17] or by optical (photoelectron) spectroscopy of the corresponding anion.[18–23] In the case of optical spectroscopy of the anion: Schiedt and Weinkauf used photodetachment and PE spectroscopy on jet-cooled anthracene and its complex with a single water molecule;[21] Song *et al.* studied anionic clusters of anthracene $(C_{14}H_{10})_n^-$ (n = 1–16) by PE spectroscopy;[22] and more recently, Kregel *et al.* presented a very high resolution slow-electron PE imaging of $C_{14}H_{10}^-$.[23] The PE spectra by Song *et al.* at wavelengths of 532 nm, 610 nm, and 700 nm contained evidence of indirect detachment features that were redshifted relative to the direct detachment (DD) peak accessing the neutral ground state.[22] The spectral range over which this indirect band appeared was consistent with the vertical excitation energy reported for a π^* resonance, from which autodetachment can occur.

While individual PE spectra can inform on the presence of a resonance, they do not encapsulate trends and overall patterns of resonances and their dynamics. To that end, we have developed 2D PE spectroscopy as a general method to identify such trends and dynamical fingerprints.[24] As an optical analog of 2D electron energy loss spectroscopy,[25–28] it also provides a direct link to electron spectroscopy, particularly in cases where the anion and neutral geometries are similar, as may be expected for anthracene. Several electron impact resonances of a number of PAHs including anthracene have been observed in electron transmission spectra.[16]

The electronic structure and excited states of $C_{14}H_{10}^-$ have also been considered computationally using electronic structure methods, but because of its size and open-shell electronic structure, the number of these have been limited.[29–32] The size of $C_{14}H_{10}^-$ lends itself well to Density Functional Theory (DFT) calculations and provides a platform for extending to larger PAHs. However, open-shell anionic species have traditionally proved more challenging to compute than their neutral counterparts.[33] Dessent used anthracene as a test molecule in a DFT benchmark study of the ground state vibrational properties of the neutral and anion,[29] and Kreger *et al.* showed good agreement between their DFT calculations and vibrational structure in the high-resolution PE spectra.[23] Malloci *et al.* focused on the electronic properties of the anion and computed the five lowest energy resonances as part of a wider Time-Dependent DFT (TDDFT) study of charged PAHs.[31] In the present study, we use TDDFT calculations to support the interpretation of the 2D PE spectroscopy of $C_{14}H_{10}^-$. The calculations are aimed to provide qualitative insight and capture the overall electronic structure of the observed resonances. Our work shows that, while there are several low-lying resonances that can lead to the formation of a temporary negative ion, there is only a small amount of ground electronic state recovery, suggesting that the lifetimes for autodetachment are relatively short and that anthracene by itself is not likely to form $C_{14}H_{10}^-$ upon low energy electron impact.

II. EXPERIMENTAL AND COMPUTATIONAL DETAILS

A description of the experimental setup has been presented in detail elsewhere,[34] and only an outline is provided here. Solid anthracene (Sigma-Aldrich) was heated at 180 °C in an Even–Lavie valve,[35] and the resulting molecular vapor was expanded through the pulsed valve into vacuum using Ar as a carrier gas (5 bar). The molecular beam expansion was intersected by an electron beam (300 eV) at the throat of the expansion, forming $C_{14}H_{10}^-$ and its clusters, $(C_{14}H_{10})_n^-$. An ion packet containing $C_{14}H_{10}^-$ was mass-selected using a Wiley–Mclaren time-of-flight spectrometer.[36] At the focus of the mass-spectrometer, the ion packet was intersected by nanosecond laser pulses from a tunable Nd:YAG pumped optical parametric oscillator. The resulting photodetached electrons were analyzed using a velocity map imaging spectrometer.[37] The polar onion-peeling algorithm was used in the reconstruction of the PE spectra from raw images.[38] The electron kinetic energy (eKE) axis for the PE spectra was calibrated using the known PE spectrum of I^-, and spectra have a resolution of $\Delta eKE/eKE \sim 3\%$.

To aid the characterization of anion resonances, DFT and TDDFT calculations were employed. DFT optimization calculations were performed on the open-shell anthracene anion at the B3LYP/6-311++G level of theory using Gaussian09.[39–42] This level of theory has been shown to reproduce experimental parameters accurately.[29,43] The minimum energy structure of the anthracene anion was confirmed using vibrational analysis. Computation of the neutral optimized geometry and the neutral at the anion geometry were also performed at the same level of theory to permit the theoretical determination of the adiabatic and vertical detachment energies, respectively. Following this, the lowest 50 excited states of anionic anthracene were computed using TDDFT at the previously stated level of theory.

The calculation of anion resonance states is complicated by excited states describing electron loss from the anion, i.e., discretized continuum states (DCSs).[43] Resonances must be distinguished from DCS, which we do here using the basis set stabilization method.[44] This involves the incremental variation of the diffuseness of the basis; the energy of resonances is insensitive to this diffuseness, while the energies of DCSs decrease rapidly with the increase in basis set size.[45,46] In this study, the stabilization method was implemented using the 6-311++G basis set, in which diffuse functions were added to both carbon and hydrogen atoms. Both diffuse exponents were scaled between 45% and 100% of their initial values in 5% increments. TDDFT calculations were performed at each exponent value, in which the first 50 excited states were computed.

III. RESULTS AND ANALYSIS

A. 2D photoelectron spectrum and angular distributions

Figure 1(a) shows the 2D PE spectrum of $C_{14}H_{10}^-$. The 2D map is composed of 137 individual PE spectra taken at 25 meV photon energy intervals in the range $0.8 < h\nu < 4.3$ eV, and each spectrum has been normalized to its total (integrated) PE signal. Hence, Fig. 1(a) shows no intensity information for different $h\nu$. In Fig. 1(b), we have reproduced the 2D PE spectrum and have annotated this with labels to aid the discussion and analysis. Figure 1(c) shows the corresponding photoelectron angular distributions, $I(\theta)$, that are quantified by the anisotropy parameter, β_2. β_2 is defined through $I(\theta) \propto 1/2\ \beta_2(3\cos^2\theta - 1)$, where θ is the angle between the electron ejection velocity vector and the polarization axis, which is fixed in the laboratory frame.[47,48] The anisotropy parameter $\beta_2 = +2$ corresponds to a $\cos^2\theta$ distribution and $\beta_2 = -1$ corresponds to a $\sin^2\theta$ distribution.

Figure 1 contains direct detachment (DD) features, which appear as diagonal features, for which the eKE increases with an increase in $h\nu$ [gradient $d(h\nu)/d(\text{eKE}) = 1$], as well as indirect autodetachment features (AD), which appear red-shifted relative to the DD features. Three distinct DD features are clearly visible. Extrapolation of these to eKE = 0 eV yields onset energies of 0.53 eV, 2.40 eV, and 4.05 eV, and we label these direct detachment channels as DD_1, DD_2, and DD_3, respectively, in Fig. 1(b).

In addition to the DD channels, a number of AD features are shown in Fig. 1(a) and are highlighted in Fig. 1(b). The eKE associated with the AD feature appears mostly independent of photon energy (vertical features in the 2D PE spectrum). The clearest AD features are AD_1, AD_3, and AD_4, which can be readily identified from Fig. 1(a). In contrast, the feature AD_2 warrants a more careful

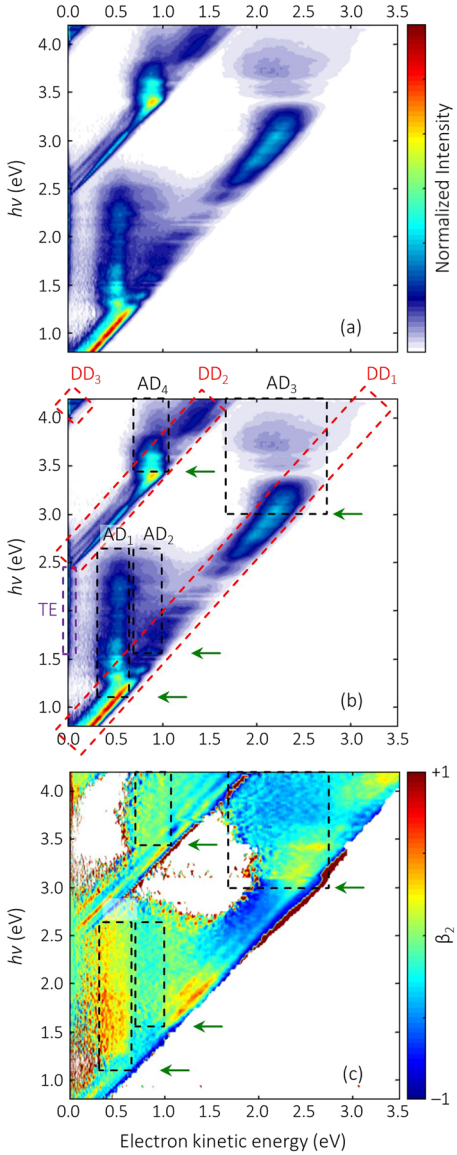

FIG. 1. (a) 2D PE spectrum of $C_{14}H_{10}^-$, normalized to the integrated intensity of each spectrum. (b) Annotated version of (a) that includes labels of the various accessible detachment channels: direct detachment (DD), autodetachment (AD), and thermionic emission (TE). (c) 2D β_2 spectra associated with the 2D PE spectra in (a) and (b), with AD regions highlighted. Regions where the PE signal is too low to confidently assign a β_2 value are left white. The location of resonances derived from the experiment (see text) is shown by green horizontal arrows.

consideration. There are a number of points that lead us to conclude that feature AD_2 is independent of AD_1. First, there is a distinct AD feature to higher eKE than that of AD_1. Figure 2 shows an example PE spectrum taken at $h\nu$ = 2.30 eV, including a deconvolution of the spectrum into three separate Gaussian functions representing AD_1, AD_2, and DD_1. This clearly shows the additional signal associated with AD_2. The second point of evidence is the peak at eKE = 0 eV, clearly visible in Fig. 2 (though not included in the

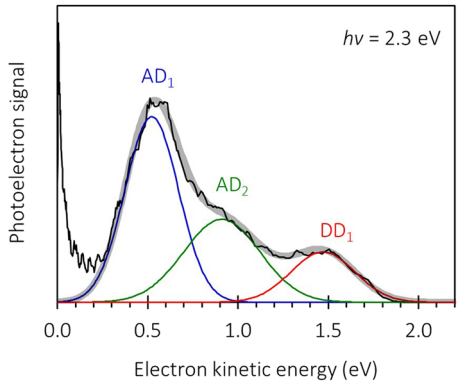

FIG. 2. Photoelectron spectrum of $C_{14}H_{10}^-$ taken at $h\nu$ = 2.30 eV. Direct and indirect features are indicated and correspond to the regions shown in Fig. 1(b). The spectrum has been fitted to three Gaussian functions to represent features AD_1 (blue line), AD_2 (green line), and DD_1 (red line). The sum of these contributions is overlaid as a thick gray line.

deconvolution). This peak is labeled TE in Fig. 1(b) and does not coincide with the $h\nu$ at which AD_1 appears. Instead, the TE signal only turns on at $h\nu > 1.6$ eV, which is where AD_2 appears to start contributing also. Finally, there is further evidence in the 2D β_2

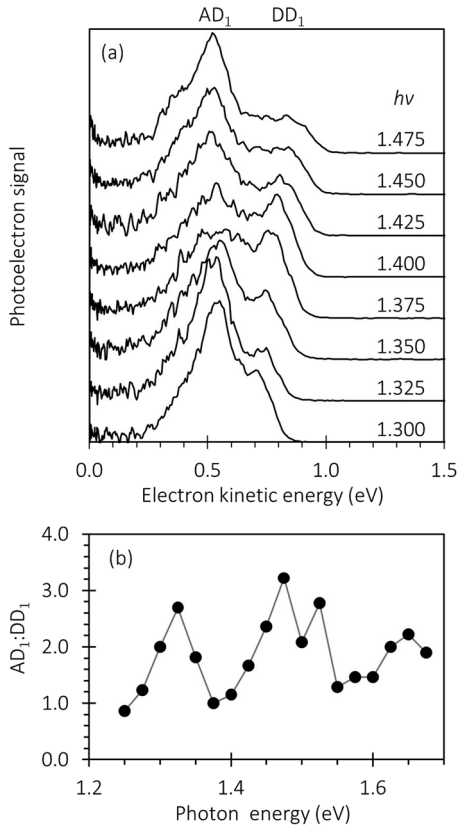

FIG. 3. (a) Photoelectron spectrum of $C_{14}H_{10}^-$ taken at a series of photon energies where both direct and indirect features [DD_1 and AD_1 in Fig. 1(b)] are visible. (b) Ratio of peak heights of AD_1:DD_1 as a function of photon energy.

spectrum, which is shown in Fig. 1(c) in the range $-1 < \beta_2 < +1$ to accentuate changes. Specifically, it is expected that β_2 remains mostly constant or at least is slowly varying as a function of eKE. Instead, it is clear from Fig. 1(c) that β_2 associated with AD_1 differs from that of AD_2. For example, for $h\nu = 2.30$ eV (PE spectrum shown in Fig. 2), β_2 for AD_1 is positive, while that for AD_2 is negative, suggesting different electronic states are responsible for these electron emission channels.

To determine the onset at which a given AD channel appears, we have extrapolated their vertical PE features to the point where they intersect with the corresponding DD feature. Using this approximate method, the onsets of the AD channels are found to be at photon energies corresponding to $h\nu \sim 1.1$ eV, 1.6 eV, 3.0 eV, and 3.4 eV for AD_1, AD_2, AD_3, and AD_4, respectively. These estimated onsets are indicated by the horizontal green arrows in Fig. 1(b). These onsets can also be identified in the 2D β_2 spectrum. Abrupt changes in β_2 as a function of $h\nu$ are not expected for DD features, unless a resonance is excited,[49–52] and such changes imply excitation of resonances in the 2D β_2 spectrum. For example, if one takes an average of β_2 across the DD_1 diagonal feature in Fig. 1(c), then clear changes can be seen at $h\nu \sim 1.6$ eV: just below this energy, β_2 of DD_1 is negative and just above it, β_2 of DD_1 has become positive. Hence, at $h\nu \sim 1.6$ eV, a resonance is excited and this resonance coincides with the appearance of AD_2. A similar abrupt change can be seen around $h\nu \sim 3.0$ eV, where β_2 rapidly changes from negative to positive with an increase in $h\nu$. This change can be associated with the appearance of AD_3.

Figure 3(a) shows a series of PE spectra taken between $h\nu = 1.30$ eV and 1.45 eV that are representative of the region where the AD_1 indirect channel contributes. This clearly shows the redshift of the AD_1 channel with respect to the corresponding DD_1 channel. However, Fig. 3(a) shows that the ratio between AD_1 and DD_1 is not constant. For example, at $h\nu = 1.30$ eV and 1.45 eV, the ratio of the PE signal AD_1:DD_1 is greater than at $h\nu = 1.38$ eV. Indeed, there is a modulation of the PE signal associated with the AD_1 channel that is out-of-phase with a similar modulation in the DD_1 channel. This modulation can also be seen in the 2D PE spectrum in Fig. 1(a). To provide a rough analysis of this modulation, we have calculated the ratio of the peak intensity of the AD_1 and DD_1 feature. Figure 3(b) shows the result of this analysis and clearly recovers the oscillation in AD_1:DD_1. The peaks in Fig. 3(b) are spaced approximately 150 meV. Evidence of similar oscillations is also shown in AD_3 and AD_4 in Fig. 1(a), but these are less obvious and we refrain from analyzing these channels in a similar manner.

B. Computational

The ground state of $C_{14}H_{10}^-$ has D_{2h} symmetry. The symmetry labels are derived assuming that anthracene lies in the y-z plane with the z-axis being the long molecular axis. The relevant MOs are shown in Fig. 4. $C_{14}H_{10}^-$ has an electronic configuration $\ldots\pi(b_{1g})^2\,\pi(b_{3u})^1$, corresponding to a ground $^2B_{3u}$ state. The two lowest neutral states are also included in Fig. 4. Loss of the electron in the singly occupied MO (SOMO) of b_{3u} symmetry leads to the neutral ground $X\,^1A_g$ state. The lowest triplet state of the neutral has a $\ldots\pi(b_{1g})^1\pi(b_{3u})^1$ configuration leading to a $^3B_{2u}$ state.

Figure 5 shows the results from the TDDFT calculations over a range of basis set diffuseness, where the exponent value is inverse to the diffuseness. Most excited states are observed to vary in transition energy as the exponent (diffuseness) changes. The states that rapidly change in energy as a function of diffuseness are associated with DCSs (as the diffuseness describes the effective "box" size that the orbitals can occupy, L, the energy of the DCSs will scale approximately as L^{-2}). However, some of the states appear to deviate from this trend and are constant in energy over limited ranges of the basis set diffuseness. An example of one such state is highlighted in green in Fig. 5. In the range where the energy is not changing significantly, the DCS has taken on the character of a resonance and remains so

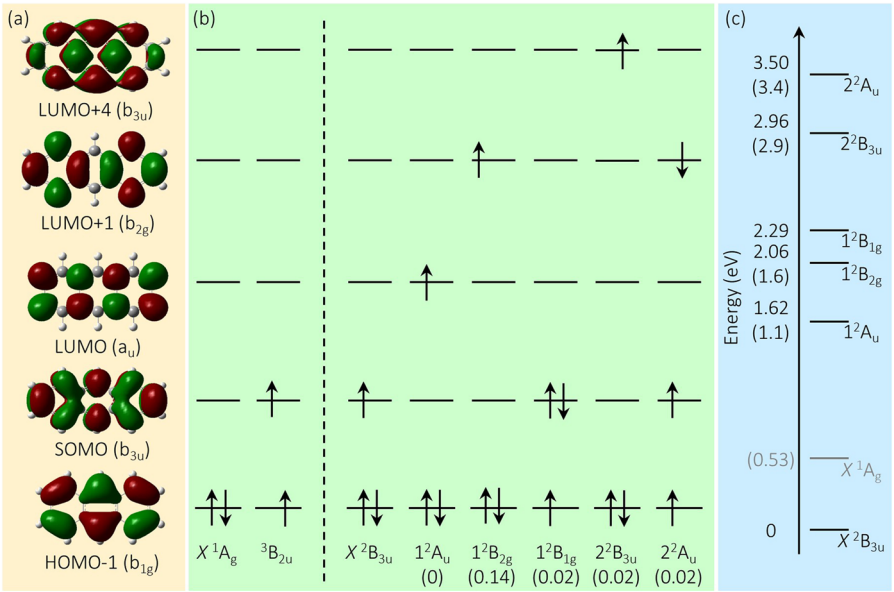

FIG. 4. (a) Frontier molecular orbitals (MOs) of $C_{14}H_{10}^-$. (b) Electronic configuration of neutral ground and triplet excited states and electronic configurations of radical anion and lowest-lying resonances, with optical excitation oscillator strength given in brackets. (c) Energy level diagram of relevant calculated excited states of the anion (black) and neutral (gray), with experimental energies from this study given in brackets. All energies are in eV.

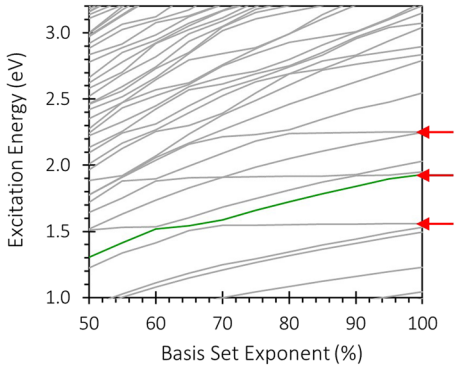

FIG. 5. Stabilization plot of the excited state energies (gray lines) as a function of basis set exponent [small values (%) refer to diffuse basis sets]. Horizontal arrows indicate the location of resonances, with the lowest three clearly visible. The green solid line shows an adiabatic evolution of the state's character with basis set diffuseness and shows the changes from discretized continuum states to valence states.

until it undergoes an avoided crossing with another DCS, at which point the resonance will take on the character of that DCS. Despite the series of (avoided) crossings between the states, there are clear regions over which a resonance can be identified at a given excitation energy. These are highlighted in Fig. 5 by horizontal arrows.

Figure 4 includes the excited states (energies and corresponding oscillator strength) and the associated electronic configuration based on the relevant MOs. These were computed using a 6-311G basis set, which is effectively the upper limit of the TDDFT calculations in which the exponent reaches infinity and there are no diffuse functions present. The lowest energy resonance, 1^2A_u, corresponds to the excitation of an electron in the SOMO (b_{3u}) to the LUMO (a_u) and has a calculated oscillator strength of zero (symmetry forbidden). This is followed by two close-lying resonances, 1^2B_{2g} and 1^2B_{1g}, that correspond to transitions from LUMO + 1 ← SOMO and SOMO ← HOMO − 1, respectively. $1^2B_{2g} \leftarrow X\ ^2B_{3u}$ has the largest oscillator strength. At higher energy, resonances are more difficult to assign because of a much higher density of DCSs. Nevertheless, we can identify regions that are relatively constant in energy just below 3 eV in Fig. 5. These correspond to the transitions shown in Fig. 4 that access the 2^2B_{3u} and 2^2A_u states.

IV. DISCUSSION

A. Assignment of direct detachment channels

The adiabatic detachment energy (ADE) of $C_{14}H_{10}^-$ has been determined by Kregel and co-workers using high-resolution slow electron velocity map imaging (SEVI) measurements to be 0.532(3) eV, and the adiabatic detachment energy to reach the first triplet state was found to be 2.404(3) eV.[23] These are in agreement with the onset of the DD_1 channel at 0.53 eV and the DD_2 channel at 2.40 eV and allows us to assign DD_1 to $X\ ^2B_{3u} + h\nu \rightarrow X\ ^1A_g + e^-$ and DD_2 to $X\ ^2B_{3u} + h\nu \rightarrow\ ^3B_{2u} + e^-$. Channel DD_3 corresponds to the excitation of the neutral to its first singlet excited state in the photodetachment: $X\ ^2B_{3u} + h\nu \rightarrow\ ^1B_{2u} + e^-$. This assignment is in agreement with the gas-phase absorption spectrum of neutral anthracene, which has its 0–0 transition of the $^1B_{2u} \leftarrow X\ ^1A_g$ band at 3.42 eV.[53,54] Based on this, the DD_3 channel is expected to appear at $h\nu$ = 3.95 eV in the present experiment, in reasonable agreement with our measurement of 4.05 eV.

The DD_1 and DD_2 channels show some vibrational structure in the 1D PE spectra, which corresponds to the vibrational modes of the ground electronic state of the neutral and its first triplet excited state, respectively. These vibrational levels of the neutral have been discussed in detail by Kregel and co-workers,[23] whose experiment is of much higher resolution than ours, and so, we will not discuss these further.

B. Assignment of resonances

There are several accessible resonances in the spectral range probed here, but there are no bound excited states of $C_{14}H_{10}^-$. From the experiment, we estimate the location of the two lowest-lying resonances to be at approximately $h\nu \sim 1.1$ eV and 1.6 eV (see Fig. 1). The first of these is clearly identifiable by the appearance of the autodetachment feature AD_1. The second resonance also leads to autodetachment (AD_2), but this is not as clear as the AD_1 channel. It is more apparent in the 2D β_2 spectrum in Fig. 1(c), where at 1.6 eV, there is a very clear and abrupt change in β_2. Additionally, AD_2 is distinguishable from AD_1 by its different β_2. Such qualitative changes highlight different molecular orbitals involved in the autodetachment, although obtaining quantitative information is not yet possible using current theoretical methods.

The resonances can be assigned using our calculations and those of others, as well as the absorption spectrum and electron transmission spectra. Shida and Iwata measured an absorption spectrum of $C_{14}H_{10}^-$ in a methyl-tetrahydrofuran matrix at 77 K,[19,20] which is reproduced here in Fig. 6. This shows a weak transition around $h\nu \sim 1.4$ eV with a series of vibrational peaks separated by ~ 150 meV. A second, brighter excited state was seen starting at $h\nu$ = 1.67 eV. At higher $h\nu$ (~2.1 eV), there are a series of vibrational peaks and possibly a third absorption, but the absorption spectrum is too congested to be certain of this.

The weak and low energy absorption in Fig. 6 was only collected for $h\nu > 1.3$ eV. Hence, there is a possibility that the 0–0 transition of this weak band was not observed by Shida and Iwata.

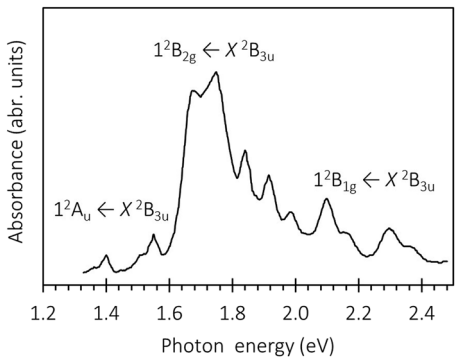

FIG. 6. Absorption spectrum of $C_{14}H_{10}^-$ in a methyl-tetrahydrofuran matrix at 77 K. Reproduced with permission from Shida and Iwata, J. Chem. Phys. **56**, 2858 (1972). Copyright 1972 AIP Publishing LLC.

This would then be consistent with the onset of the AD_1 channel that we observed at ~ 1.1 eV. It is of course also possible that the transition energies in the absorption spectrum in Fig. 6 have shifted slightly because of the presence of the matrix. The second brighter transition at 1.67 eV is not readily discerned from the 2D PE spectrum, but there is evidence that changes in the resonance dynamics are occurring. First, there is evidence that a new autodetachment signal is appearing starting from around $h\nu > 1.6$ eV (AD_2). As this signal remains constant in kinetic energy, it is clear that the relative contribution of the direct channel (DD_1) becomes less pronounced beyond $h\nu \sim 2$ eV. Second, a new indirect channel at very low energy (labeled TE) switches on for photon energies just above $h\nu \sim 1.6$ eV, suggesting that a new resonance contributes. Finally, as mentioned above, the 2D β_2 spectra clearly show a sudden change in the β_2 values associated with the DD_1 channel. Our determination of the resonance positions is in agreement with the electron transmission spectra of Burrow *et al.*,[17] who noted two π^* resonances at 0.6 eV and 1.13 eV (corresponding to $h\nu = 1.13$ eV and 1.66 eV), and with their calculations.[55–57]

The overall picture from the absorption, electron transmission, and 2D PE spectrum is qualitatively supported by our calculations. The lowest resonance is calculated at a transition energy of $h\nu = 1.62$ eV with no oscillator strength, followed by a bright resonance at $h\nu = 2.06$ eV and a third resonance at $h\nu = 2.29$ eV. These can be compared with experimental values of 1.1 eV and 1.6 eV, and the absorption spectrum that suggests that the lowest transition is weak followed by a brighter transition. The TDDFT calculations appear to overestimate the transition energies by some way (about 0.5 eV), which is not entirely surprising, given the level of our calculations,[57] but have captured the state ordering and relative energy spacing between the exited states quite well.

Based on this, we can confidently assign most resonances. The first resonance that leads to AD_1 in Fig. 1(b) is the 1^2A_u resonance. The second resonance that results in the AD_2 signal can be assigned to the 1^2B_{2g} resonance. Both the resonances are of shape character and may be expected to lead to efficient and very fast autodetachment.[56,57] The discrepancy between the observed and computed oscillator strength of 0 for the $1^2B_{2g} \leftarrow X\ ^2B_{3u}$ transition could arise from Herzberg–Teller coupling that has not been accounted for in the calculation. Based on our calculations, the third resonance predicted at $h\nu = 2.29$ eV corresponds to a $1^2B_{1g} \leftarrow X\ ^2B_{3u}$ transition. The 1^2B_{1g} resonance is of Feshbach character with respect to the $X\ ^1A_g$ neutral ground state. Hence, the lifetime of this resonance with respect to electron loss may be expected to be longer. Burrow *et al.* observed this resonance in the electron transmission spectra at 1.62 eV,[17] which would correspond to $h\nu = 2.15$ eV in the 2D PE spectrum. Indeed, this is where the vibrational structure changes in the absorption spectrum (Fig. 6).[19] In the 2D PE spectra, there is no clear indication of this resonance [see Figs. 1(a) and 1(b)]. The 2D β_2 spectra do show an abrupt change in β_2 for the DD_1 channel at $h\nu = 2.15$ eV, indicating that a different excitation is contributing. However, while the 1^2B_{1g} appears to be populated, there is no evidence that it shows differing dynamics to that observed for the 1^2A_u and 1^2B_{2g} resonances.

The higher lying resonances are predicted to the 2^2B_{3u} and 2^2A_u resonances. 2^2B_{3u} is a shape resonance, while 2^2A_u is a Feshbach resonance (Fig. 4): Loss of an electron from the b_{2g} orbital for the 2^2A_u resonance forms the neutral triplet $^3B_{2u}$ state. The 2D PE spectrum is consistent with this assignment. The lower 2^2B_{3u} resonance that leads to the AD_3 signal has a higher propensity to form the neutral $X\ ^1A_g$ ground state even though the $^3B_{2u} + e^-$ channel is energetically accessible. In contrast, the AD_4 feature is associated with the $^3B_{2u} + e^-$ channel, suggesting that the resonance leading to AD_4 is a Feshbach resonance with respect to the $X\ ^1A_g$ ground state but a shape resonance with respect to the $^3B_{2u}$ final state. This is consistent with the resonance 2^2A_u calculated at $h\nu = 3.52$ eV (see Fig. 4).

The abovementioned arguments are predominantly based on experimental ones that are qualitatively supported by our TDDFT calculations. We have specifically refrained from performing higher-level calculations to demonstrate the synergy between the experiment and TDDFT calculations and the insight these offer without the need to resort to such methods.

C. Competition between direct detachment and resonance excitation

Figure 3 shows a modulation of the ratio of PE signal in the AD_1 vs DD_1 channels. Because the 2D PE spectral intensity has been normalized relative to the integrated intensity of each spectrum, the modulation seen in Fig. 3 is a relative measure rather than an absolute measure. The absorption spectrum of $C_{14}H_{10}^-$ measured by Shida and Iwata (Fig. 6) shows the absorption band of the weak $1^2A_u \leftarrow X\ ^2B_{3u}$ transition.[19] While the origin (0–0 transition) of the band was probably not measured, a vibrational progression with a spacing of ~150 meV was observed. The oscillation in Fig. 3(b) has a similar spacing (approximately 150 meV), suggesting that the same vibrational progression in the 1^2A_u resonance is responsible for the observed oscillation. Any discrepancy between the frequencies may be due to the fact that the absorption spectrum was acquired in a matrix, which will impact the frequencies. The oscillation in Fig. 3 can thus be interpreted as an increase in cross section for excitation to the 1^2A_u state when it is resonant with specific vibrations, which in turn leads to the enhancement in AD_1 on top of a constant (or at least smoothly varying) background associated with the DD_1 channel. Oscillations in the AD:DD ratio are also seen for the higher lying resonances (AD_3 and AD_4), but these have been less well resolved.

The modulation between direct and indirect detachment as a function of $h\nu$ has been noted in the photoelectron spectra of other anionic molecules. For example, Lyle and co-workers observed changes in the cross section in the PE spectra of CuF_2^-,[58] and Masonand co-workers recently noted interesting oscillations in the PE spectra of Sm_2O^-.[59] We have also previously seen such oscillations for larger organic compounds and clusters.[60,61]

D. Spectral shape of autodetachment spectra and resonance dynamics

A particularly striking feature of AD_1 is its rather narrow spectral shape. This is shown more clearly in Fig. 2 that presents the PE spectrum taken at $h\nu = 2.30$ eV. The feature AD_1 is associated with autodetachment from the 1^2A_u resonance, and it is apparent as soon as this channel becomes accessible (see Fig. 1). The 1^2A_u resonance is of shape character, and autodetachment may be expected to be very fast. However, scattering calculations have indicated that the autodetachment lifetime of this resonance is in fact quite long–on

the order of ~100 fs.[56,57] During this relatively long autodetachment lifetime, some nuclear motion can take place on the 1^2A_u potential energy surface. Nevertheless, the electron emission is predominantly dictated by the Franck–Condon factors of the $1^2A_u \rightarrow X\ ^1A_g + e^-$ channel. The relatively narrow distribution of AD_1 then suggests that the 1^2A_u potential energy surface is quite similar to that of the $X\ ^1A_g$ final state of the neutral. The fact that the AD_1 feature does not change much with $h\nu$ suggests that the additional vibrational energy imparted in the 1^2A_u resonance upon excitation is conserved in the $X\ ^1A_g$ final state, leading to a constant eKE with an increase in $h\nu$. A similar argument was made by Bochenkova *et al.* in the analysis of the autodetachment from resonances in the green fluorescent protein chromophore anion.[62,63] By inspection of the MOs involved (Fig. 5), AD_1 corresponds to loss of an electron from the LUMO, which is antibonding only along the short axis of the molecule and non-bonding along the long axis. Hence, it is reasonable to suggest that the geometric difference between 1^2A_u and $X\ ^1A_g$ may be relatively small.

It is quite striking that the AD_1 channel persists even when the brighter $^2B_{2g}$ resonance is excited at $h\nu > 1.6$ eV, as shown in the PE spectrum at $h\nu = 2.30$ eV in Fig. 2. While there is an additional indirect signal, as exemplified by the region AD_2 in Fig. 2, the predominant signal remains in the AD_1 channel. Similarly, if the 1^1B_{1g} resonance is also populated, this appears to not have an impact on the presence and shape of the AD_1 feature.

There are two possible explanations that would be consistent with the fact that AD_1 dominates even though the 1^2B_{2g} resonance is populated. First, the 1^2B_{2g} (and perhaps also 1^2B_{1g}) resonance could undergo internal conversion to form the 1^2A_u resonance, which subsequently undergoes autodetachment to yield AD_1. Such ultrafast internal conversion processes have previously been observed in anion resonances[64,65] and are likely to be especially efficient when the potential energy surfaces involved are energetically close at the excitation Franck–Condon geometry so that only small nuclear displacements are required to lead to a conical intersection. The concept is analogous to Kasha's rule,[66] where instead of fluorescence occurring from the lowest lying excited state, autodetachment occurs from the lowest lying resonance. A second scenario to explain why the AD_1 yield is higher than AD_2 could be that the 1^2B_{2g} resonance can internally convert to the ground electronic state of the anion ($X\ ^2B_{3u}$). In this case, a reduced amount of autodetachment would be seen from the 1^2B_{2g} resonance (i.e., reduced AD_2). Instead, the $X\ ^2B_{3u}$ state is formed with a large amount of internal energy and the excess electron can subsequently be emitted statistically by thermionic emission (TE). The signature of TE is the PE signal at very low eKE (peaking at 0 eV) and with an exponentially decaying spectral profile.[67–69] Such a feature can indeed be seen in Fig. 2, and inspection of Fig. 1 shows a small TE feature that turns on at ~1.6 eV, which is consistent with the resonance energy of 1^2B_{2g} determined by extrapolation of the AD_2 feature. Hence, the TE peak correlates with the production of 1^2B_{2g}, indicating that at least a fraction of the population can reform the $X\ ^2B_{3u}$ ground state of the anion, although probably not all as AD_2 and AD_1 signals are also observed. However, both Gallup and Carelli *et al.* concluded that the autodetachment lifetime for the 1^2B_{2g} resonance is much shorter than that for the 1^2A_u resonance (by a factor of ~8).[56,57] Hence, any internal conversion dynamics must be competitive with this short lifetime. To determine the exact dynamics would require time-resolved PE spectroscopic studies. We have attempted such studies for the current system at a range of different pump and probe photon energies, but these have been frustratingly unsuccessful. Apparently, the cross sections for photodetachment from the resonances are very low.

The higher-lying resonance, 2^2B_{3u}, leads to a very broad autodetachment peak, AD_3 (Fig. 1). This could reflect very fast autodetachment from a resonance that has a very different geometry, leading to a broad range of Franck–Condon factors, or slower dynamics in which nuclear dynamics can take place on the excited state and autodetachment occurs along a range of different geometries. Because this shape resonance is at high energy, the final orbital to which the SOMO electron is excited is of greater antibonding character (see Fig. 4) so that the difference in geometry between this resonance and the $X\ ^1A_g$ ground state will probably be very large. This is consistent with the broad spectral width of AD_3. Moreover, scattering calculations suggest an extremely short lifetime (<10 fs) for autodetachment from the 2^2B_{3u} resonance,[57] which would also be consistent with the observed width of AD_3 and with the fact that no internal conversion to the lower-lying resonances is observed in Fig. 1.

E. Relevance to electron capture in the interstellar medium

As commented on in the Introduction, PAHs are an important store of carbon in the interstellar medium (ISM) and anions of PAHs have been speculated on as potentially important chemical species.[14] Here, we have shown that only the 1^2B_{2g} resonance at ~1.1 eV above the $X\ ^1A_g$ neutral ground state shows evidence of the ground state ($X\ ^2B_{3u}$) formation of the anion following electron impact. However, the temperature in the ISM is typically in the 10–30 K range and electrons are effectively thermalized to this background, suggesting that these actually have very low energies and generally below 1.1 eV.[70] Hence, it is unlikely that the 1^2B_{2g} resonance, or any other resonances in the first few eV of the electronic continuum, has any significance in the ISM and that anthracene radical anions are present. A similar conclusion was reached for the deprotonated (closed-shell) anthracenyl anion,[50] for which the 2D PE spectroscopy found no evidence for anion ground state recovery. In contrast, the tetracenyl anion did show strong thermionic emission, although the PE spectroscopy on this system suffered from poor signal to noise ratio.[71] It would certainly be of interest to study tetracene and larger acene radical anions by 2D PE imaging, and we are currently pursuing these experiments. Finally, we note that most of the PAHs in the ISM exist in icy dust grains[72] and not necessarily as isolated species. Hence, one should consider how the icy environment affects the resonance dynamics, and experiments probing the effect of incremental solvation by water molecules on the dynamics are currently underway in our laboratory.

V. SUMMARY AND CONCLUSION

The 2D photoelectron spectroscopy of the anthracene radical anion has been presented, which revealed complex and rich dynamics occurring in the anion continuum. Resonances are assigned based on previous work and TDDFT calculations. The latter show good qualitative agreement and suggest that such calculations may

be suitable when considering larger PAHs for which wavefunction-based methods become expensive. Excitation to the lowest energy resonance, 1^2A_u, shows an energy dependent competition between excitation and direct detachment that can be clearly seen in the ratio of direct to indirect electron yield. The bright 1^2B_{2g} resonance shows complex dynamics with a fraction apparently forming the 1^2A_u resonance by internal conversion and another fraction reforming the ground electronic state as evidenced by thermionic emission. At higher energy, other resonances show interesting dynamics and can be assigned based on Koopmans' correlation to the singlet and triplet states of the neutral. Overall, the dynamics show that low energy electron impact onto anthracene does not generate a large amount of ground state anions and therefore can be viewed as being rather inefficient in accepting electrons, especially in the interstellar medium.

ACKNOWLEDGMENTS

This work was funded by the EPSRC through the award of a DTP studentship (Grant No. EP/M507854/1 and Grant No. EP/R023085/1).

DATA AVAILABILITY

The data that support the findings of this study are available from the corresponding author upon reasonable request.

REFERENCES

[1] A. Rescifina, M. A. Chiacchio, A. Corsaro, E. De Clercq, D. Iannazzo, A. Mastino, A. Piperno, G. Romeo, R. Romeo, and V. Valveri, J. Med. Chem. **49**, 709 (2006).
[2] F. F. Becker and B. K. Banik, Front. Chem. **2**, 55 (2014).
[3] B. J. Finlayson-Pitts and J. N. Pitts, Science **276**, 1045 (1997).
[4] J. Huang, J.-H. Su, and H. Tian, J. Mater. Chem. **22**, 10977 (2012).
[5] M. Kitamura, T. Imada, and Y. Arakawa, Appl. Phys. Lett. **83**, 3410 (2003).
[6] F. Salama, E. L. O. Bakes, L. J. Allamandola, and A. G. G. M. Tielens, Astrophys. J. **458**, 621 (1996).
[7] T. R. Geballe, J. Phys.: Conf. Ser. **728**, 062005 (2016).
[8] G. P. van der Zwet and L. J. Allamandola, in *Light Dark Matter*, edited by F. P. Israel (Springer Netherlands, 1986), pp. 233–236.
[9] A. Omont, H. F. Bettinger, and C. Tönshoff, Astron. Astrophys. **625**, A41 (2019).
[10] M. Steglich, J. Bouwman, F. Huisken, and T. Henning, Astrophys. J. **742**, 2 (2011).
[11] T. P. Snow, V. Le Page, Y. Keheyan, and V. M. Bierbaum, Nature **391**, 259 (1998).
[12] S. Lepp and A. Dalgarno, Astrophys. J. **335**, 769 (1988).
[13] F. Carelli and F. A. Gianturco, Mon. Not. R. Astron. Soc. **422**, 3643 (2012).
[14] S. L. Lunt, D. Field, S. V. Hoffmann, R. J. Gulley, and J. P. Ziesel, J. Phys. B: At. Mol. Opt. Phys. **32**, 2707 (1999).
[15] J. C. Rienstra-Kiracofe, C. J. Barden, S. T. Brown, and H. F. Schaefer, J. Phys. Chem. A **105**, 524 (2001).
[16] K. D. Jordan and P. D. Burrow, Chem. Rev. **87**, 557 (1987).
[17] P. D. Burrow, J. A. Michejda, and K. D. Jordan, J. Chem. Phys. **86**, 9 (1987).
[18] J. K. Song, N. K. Lee, and S. K. Kim, Angew. Chem., Int. Ed. **42**, 213 (2003).
[19] T. Shida and S. Iwata, J. Chem. Phys. **56**, 2858 (1972).
[20] T. Shida and S. Iwata, J. Am. Chem. Soc. **95**, 3473 (1973).
[21] J. Schiedt and R. Weinkauf, Chem. Phys. Lett. **266**, 201 (1997).
[22] J. K. Song, N. K. Lee, J. H. Kim, S. Y. Han, and S. K. Kim, J. Chem. Phys. **119**, 3071 (2003).
[23] S. J. Kregel, G. K. Thurston, and E. Garand, J. Chem. Phys. **148**, 234306 (2018).
[24] C. S. Anstöter, J. N. Bull, and J. R. R. Verlet, Int. Rev. Phys. Chem. **35**, 509 (2016).
[25] M. Allan, K. Regeta, J. D. Gorfinkiel, Z. Mašín, S. Grimme, and C. Bannwarth, Eur. Phys. J. D **70**, 123 (2016).
[26] K. Regeta and M. Allan, Phys. Rev. Lett. **110**, 203201 (2013).
[27] F. Currell and J. Comer, Phys. Rev. Lett. **74**, 1319 (1995).
[28] T. Reddish, F. Currell, and J. Comer, J. Phys **21**, 203 (1988).
[29] C. E. H. Dessent, Chem. Phys. Lett. **330**, 180 (2000).
[30] G. Malloci, G. Mulas, G. Cappellini, V. Fiorentini, and I. Porceddu, Astron. Astrophys. **432**, 585 (2005).
[31] G. Malloci, G. Mulas, G. Cappellini, and C. Joblin, Chem. Phys. **340**, 43 (2007).
[32] R. V. Khatymov, M. V. Muftakhov, and P. V. Shchukin, Rapid Commun. Mass Spectrom. **31**, 1729 (2017).
[33] M.-C. Kim, E. Sim, and K. Burke, J. Chem. Phys. **134**, 171103 (2011).
[34] J. P. Rogers, C. S. Anstöter, J. N. Bull, B. F. E. Curchod, and J. R. R. Verlet, J. Phys. Chem. A **123**, 1602 (2019).
[35] U. Even, J. Jortner, D. Noy, N. Lavie, and C. Cossart-Magos, J. Chem. Phys. **112**, 8068 (2000).
[36] W. C. Wiley and I. H. McLaren, Rev. Sci. Instrum. **26**, 1150 (1955).
[37] A. T. J. B. Eppink and D. H. Parker, Rev. Sci. Instrum. **68**, 3477 (1997).
[38] G. M. Roberts, J. L. Nixon, J. Lecointre, E. Wrede, and J. R. R. Verlet, Rev. Sci. Instrum. **80**, 053104 (2009).
[39] A. D. Becke, J. Chem. Phys. **98**, 5648 (1993).
[40] A. D. McLean and G. S. Chandler, J. Chem. Phys. **72**, 5639 (1980).
[41] R. Krishnan, J. S. Binkley, R. Seeger, and J. A. Pople, J. Chem. Phys. **72**, 650 (1980).
[42] M. Frisch, G. Trucks, H. Schlegel, G. Scuseria, M. Robb, J. Cheeseman, G. Scalmani, V. Barone, B. Mennucci, G. Petersson, H. Nakatsuji, M. Caricato, X. Li, H. Hratchian, A. Izmaylov, J. Bloino, G. Zheng, J. Sonnenberg, M. Hada, M. Ehara, K. Toyota, R. Fukuda, J. Hasegawa, M. Ishida, T. Nakajima, Y. Honda, O. Kitao, H. Nakai, T. Vreven, J. Montgomery, J. Peralta, F. Ogliaro, M. Bearpark, J. Heyd, E. Brothers, K. Kudin, V. Staroverov, R. Kobayashi, J. Normand, K. Raghavachari, A. Rendell, J. Burant, S. Iyengar, J. Tomasi, M. Cossi, N. Rega, J. Millam, M. Klene, J. Knox, J. Cross, V. Bakken, C. Adamo, J. Jaramillo, R. Gomperts, R. Stratmann, O. Yazyev, A. Austin, R. Cammi, C. Pomelli, J. Ochterski, R. Martin, K. Morokuma, V. Zakrzewski, G. Voth, P. Salvador, J. Dannenberg, S. Dapprich, A. Daniels, Farkas, J. Foresman, J. Ortiz, J. Cioslowski, and D. Fox, Gaussian 09 (Gaussian, Inc., Wallingford, CT, 2009).
[43] C. W. Bauschlicher, Chem. Phys. Lett. **409**, 235 (2005).
[44] A. U. Hazi and H. S. Taylor, Phys. Rev. A **1**, 1109 (1970).
[45] J. Simons, J. Phys. Chem. A **112**, 6401 (2008).
[46] J. S. Y. Chao, M. F. Falcetta, and K. D. Jordan, J. Chem. Phys. **93**, 1125 (1990).
[47] J. Cooper and R. N. Zare, J. Chem. Phys. **48**, 942 (1968).
[48] K. L. Reid, Annu. Rev. Phys. Chem. **54**, 397 (2003).
[49] C. W. West, J. N. Bull, E. Antonkov, and J. R. R. Verlet, J. Phys. Chem. A **118**, 11346 (2014).
[50] L. H. Stanley, C. S. Anstöter, and J. R. R. Verlet, Chem. Sci. **8**, 3054 (2017).
[51] C. S. Anstöter, C. R. Dean, and J. R. R. Verlet, Phys. Chem. Chem. Phys. **19**, 29772 (2017).
[52] C. S. Anstöter, T. E. Gartmann, L. H. Stanley, A. V. Bochenkova, and J. R. R. Verlet, Phys. Chem. Chem. Phys. **20**, 24019 (2018).
[53] A. Thöny and M. J. Rossi, J. Photochem. Photobiol. Chem. **104**, 25 (1997).
[54] J. Ferguson, L. W. Reeves, and W. G. Schneider, Can. J. Chem. **35**, 1117 (1957).
[55] P. D. Burrow and G. A. Gallup, New J. Phys. **16**, 028001 (2014).
[56] G. A. Gallup, J. Chem. Phys. **139**, 104308 (2013).
[57] F. Carelli, F. A. Gianturco, M. Satta, and F. Sebastianelli, Int. J. Mass Spectrom. **365-366**, 377 (2014).
[58] J. Lyle, T.-C. Jagau, and R. Mabbs, Faraday Discuss. **217**, 533 (2019).
[59] J. L. Mason, J. E. Topolski, J. Ewigleben, S. S. Iyengar, and C. C. Jarrold, J. Phys. Chem. Lett. **10**, 144 (2019).
[60] J. N. Bull, C. W. West, and J. R. R. Verlet, Chem. Sci. **7**, 5352 (2016).
[61] J. N. Bull, C. S. Anstöter, and J. R. R. Verlet, J. Phys. Chem. A **124**, 2140 (2020).
[62] A. V. Bochenkova, B. Klaerke, D. B. Rahbek, J. Rajput, Y. Toker, and L. H. Andersen, Angew. Chem., Int. Ed. **53**, 9797 (2014).

[63]C. W. West, J. N. Bull, A. S. Hudson, S. L. Cobb, and J. R. R. Verlet, J. Phys. Chem. B **119**, 3982 (2015).
[64]J. N. Bull, C. W. West, and J. R. R. Verlet, Chem. Sci. **6**, 1578 (2015).
[65]D. A. Horke, Q. Li, L. Blancafort, and J. R. R. Verlet, Nat. Chem. **5**, 711 (2013).
[66]M. Kasha, Discuss. Faraday Soc. **9**, 14 (1950).
[67]E. E. B. Campbell and R. D. Levine, Annu. Rev. Phys. Chem. **51**, 65 (2000).
[68]J. U. Andersen, E. Bonderup, and K. Hansen, J. Phys. B: At., Mol., Opt. Phys. **35**, 2183 (2002).
[69]C. L. Adams, K. Hansen, and J. M. Weber, J. Phys. Chem. A **123**, 8562 (2019).
[70]O. Ingólfsson, *Low-Energy Electrons : Fundamentals and Applications* (Jenny Stanford Publishing, 2019).
[71]J. N. Bull, C. W. West, and J. R. R. Verlet, Phys. Chem. Chem. Phys. **17**, 32464 (2015).
[72]D. J. Burke and W. A. Brown, Phys. Chem. Chem. Phys. **12**, 5947 (2010).